PAPER

Target dependence of post-collision effects in ionization by proton impact

IOP Publishing Journal of Physics B: Atomic, Molecular and Optical Physics
J. Phys. B: At. Mol. Opt. Phys. **52** (2019) 125202 (8pp) https://doi.org/10.1088/1361-6455/ab1df5

Target dependence of post-collision effects in ionization by proton impact

A Silvus[1], M Dhital[1], S Bastola[1], J Buxton[1], Z Klok[1], E Ali[1], M F Ciappina[2], B Boggs[1], D Cikota[1], D H Madison[1] and M Schulz[1]

[1] Dept. of Physics and LAMOR, Missouri University of Science & Technology, Rolla, MO 65409, United States of America
[2] Institute of Physics of the ASCR, ELI-Beamlines, Na Slovance 2, 182 21 Prague, Czech Republic

E-mail: Schulz@mst.edu

Received 13 February 2019, revised 3 April 2019
Accepted for publication 30 April 2019
Published 28 May 2019

Abstract

We have measured and calculated double differential cross sections for ionization of Ne and Ar by 75 keV proton impact for a broad range of fixed projectile energy losses as a function of scattering angle. Along with data obtained previously for lighter targets this made possible a systematic analysis of post-collision effects between the scattered projectile and the continuum electron in the exit channel as a function of the target ionization potential. The data are consistent with an increasing strength of such effects with increasing ionization potential. However, second-order effects involving the projectile—residual target ion interaction also play an important role.

Keywords: ionization, atomic collisions, few-body problem

(Some figures may appear in colour only in the online journal)

1. Introduction

Ionization of the light targets hydrogen (atomic and molecular) and helium by ion impact has been studied extensively e.g. [1–27]. Experimental data range from total cross sections (for a review see [1]), differential ejected electron spectra e.g. [2–6], differential scattered projectile spectra e.g. [7–9], to fully differential cross sections e.g. [10–16]. Until relatively recently, theoretical studies have focused on perturbative approaches based on either the Born series e.g. [17, 18] or distorted wave methods e.g. [19–24]. The large mass of ionic projectiles makes non-perturbative calculations rather challenging because a very large number of angular momentum states of the scattered projectiles have to be accounted for. Nevertheless, in recent years, such approaches have been successfully implemented e.g. [25–27].

The overarching goal of such studies is to advance our understanding of the few-body dynamics in systems consisting of only a few charged particles. In perturbative approaches the few-body dynamics is described by expressing the transition amplitude in terms of first- and higher order contributions. There, the projectile is treated as a perturbation to the target system and an nth-order mechanism involves n interactions between the projectile and the target electrons or the target nucleus. Within such models, understanding the few-body dynamics means accurately describing the contributions from first- and the various higher-order channels.

One important higher-order mechanism which has been studied extensively e.g. [2–4, 6–8, 10–14, 16] is known as post-collision interaction (PCI). This process involves at least two interactions between the projectile and the active electron: a primary interaction lifting the electron to the continuum and a secondary interaction in the outgoing part of the collision in which both particles attract each other. This second interaction leads to an enhanced flux of electrons with a velocity close to the projectile velocity. However, it has been pointed out that a further interaction, involving the target nucleus, is required for such a focusing effect by PCI [8]. Classically, after two particles collide they will depart from each other and they can thus only collide for a second time if at least one of them gets redirected by a collision with a third particle. In target ionization by charged particle impact the third body is the residual target ion, which can either redirect the ejected electron or the projectile. Correspondingly, there are two leading-order interaction sequences which can lead to PCI effects: V_{Pe}–V_{eT}–V_{Pe} and V_{Pe}–V_{PT}–V_{Pe}, where the

subscripts P, e, and T stand for projectile, electron, and target nucleus, respectively.

Experimentally, PCI effects in ion-atom collisions were first observed in double differential electron energy spectra [2]. A sharp peak structure at an electron energy corresponding to an electron speed equal to the projectile speed, known as the 'cusp peak', was observed when electron ejection angles of 0 deg. were selected. Later, the impact of the counteraction of this PCI-focusing that the projectile exerts on the electron, namely a corresponding PCI-focusing that the electron exerts on the projectile, was observed in double differential scattered projectile spectra [6–8]. The average scattering angle θ_{ave} was measured as a function of the ejected electron energy and found to minimize near the cusp energy for atomic and molecular hydrogen targets. More recently, an even more pronounced minimum was observed in θ_{ave} extracted from fully differential cross sections in $p + H_2$ collisions when electron emission angles of 0 deg. were selected [16]. However, for a helium target instead of a minimum a significant increase in slope was found at the cusp energy [6].

The difference in θ_{ave} between hydrogen and helium suggests that PCI effects are weaker in the former than in the latter target. One difference between both species is the ionization potential I, which for helium (24.6 eV) is significantly larger than for molecular and atomic hydrogen (15.4 and 13.6 eV, respectively). This raises the question whether PCI effects tend to decrease with increasing I. Intuitively, one might expect the exact opposite trend. The extreme scenario of $I = 0$ (i.e. an unbound electron) is equivalent to the target nucleus not even being present so that neither of the two interaction sequences leading to PCI is active.

In this article we present a study of post-collisional effects in ionization of Ne and Ar by 75 keV proton impact. Along with the data obtained previously for light targets this enabled us to analyze such effects as a function of I. At the cusp energy it could not be conclusively determined whether PCI becomes more or less important with increasing I. However, for smaller ejected electron energies the data are clearly consistent with an increasing importance of PCI with increasing I. Furthermore, our calculations predict a significant dependence of PCI effects on the initial target state. However, this prediction is not fully supported by the experimental data.

Experiment

The experiment was performed at the ion-accelerator laboratory of the Missouri University of Science & Technology. A proton beam with an intrinsic energy spread of much less than 1 eV was generated using a hot cathode ion source and extracted at an energy of 5 keV. The accelerator terminal was at a voltage of about 70 kV so that the protons exited the accelerator with an energy of approximately 75 keV. The projectile beam was passed through horizontal and vertical collimating slits with a width of 150 μm and entered the target chamber, where it was crossed with a very cold Ne or Ar beam from a supersonic jet. The projectiles which did not charge exchange in the collision were selected by a switching magnet before entering a decelerator terminal, in which an electrostatic parallel-plate energy analyzer [28] was located.

The scattered protons were energy-analyzed as follows: a power supply provided a high voltage of $V_{dec} = 70$ kV to the decelerator terminal. An offset power supply delivered an output voltage V_{off} relative to the decelerator ground, which was connected to the accelerator terminal. Therefore, the exact proton energy after exiting the accelerator was $(V_{dec} + V_{off})\, e + 5$ keV (where e is the elementary charge). If in the collision with the target the projectiles suffered an energy loss of ε, the proton energy was $(V_{dec} + V_{off})\ e + 5\,\text{keV} - \varepsilon$ after the target chamber and $V_{off}\, e + 5\,\text{keV} - \varepsilon$ inside the decelerator terminal. There, the protons entered the energy analyzer, which was set for a pass energy of 5 keV. Therefore, only projectiles for which $\varepsilon = eV_{off}$ passed through the exit slit of the analyzer and were detected by a two-dimensional position-sensitive multi-channel plate detector. From the position information the projectile scattering angle θ_p was determined.

The recoiling target ions produced in the collision were extracted by a weak electric field ($\approx 6\,\text{V cm}^{-1}$) and guided onto another two-dimensional position-sensitive multi-channel plate detector, which was set in coincidence with the projectile detector. For light target atoms or molecules the position and time-of-flight information of the recoil ions can be used to determine their momentum vectors, however, for the heavier target atoms used in this experiment, especially Ar, the momentum resolution is not sufficient. Only the timing signal was used for the coincidence, which served to clean the data from background resulting e.g. from collisions with residual gas throughout the beamline. Therefore the measured quantities were the energy loss and the scattering angle of the projectiles, from which double differential cross sections (DDCS) in electron energy and projectile solid angle were obtained.

Results and discussion

In the case of the Ar target DDCS were measured for eight different energy losses in the range 30–85 eV. In figure 1 a subset of the data is shown for $\varepsilon = 30$, 54, 60, and 85 eV as a function of θ_p, which is given in the laboratory frame. Here, $\varepsilon = 60$ eV corresponds to an electron speed close to the projectile speed. The data were normalized by setting the integral of the DDCS over the projectile solid angle equal to the cross sections singly differential in ejected electron energy, which were taken from recommended values reported in [29]. The plots of figure 1 already demonstrate that the width of the scattering angular distribution at $\varepsilon = 60$ eV is substantially smaller than at the other energy losses. For example, relative to $\theta_p = 0$ the DDCS drop by one order of magnitude at θ_p less than 0.4 mrad for $\varepsilon = 60$ eV, while for the other energy losses the corresponding angle is around 0.5 mrad.

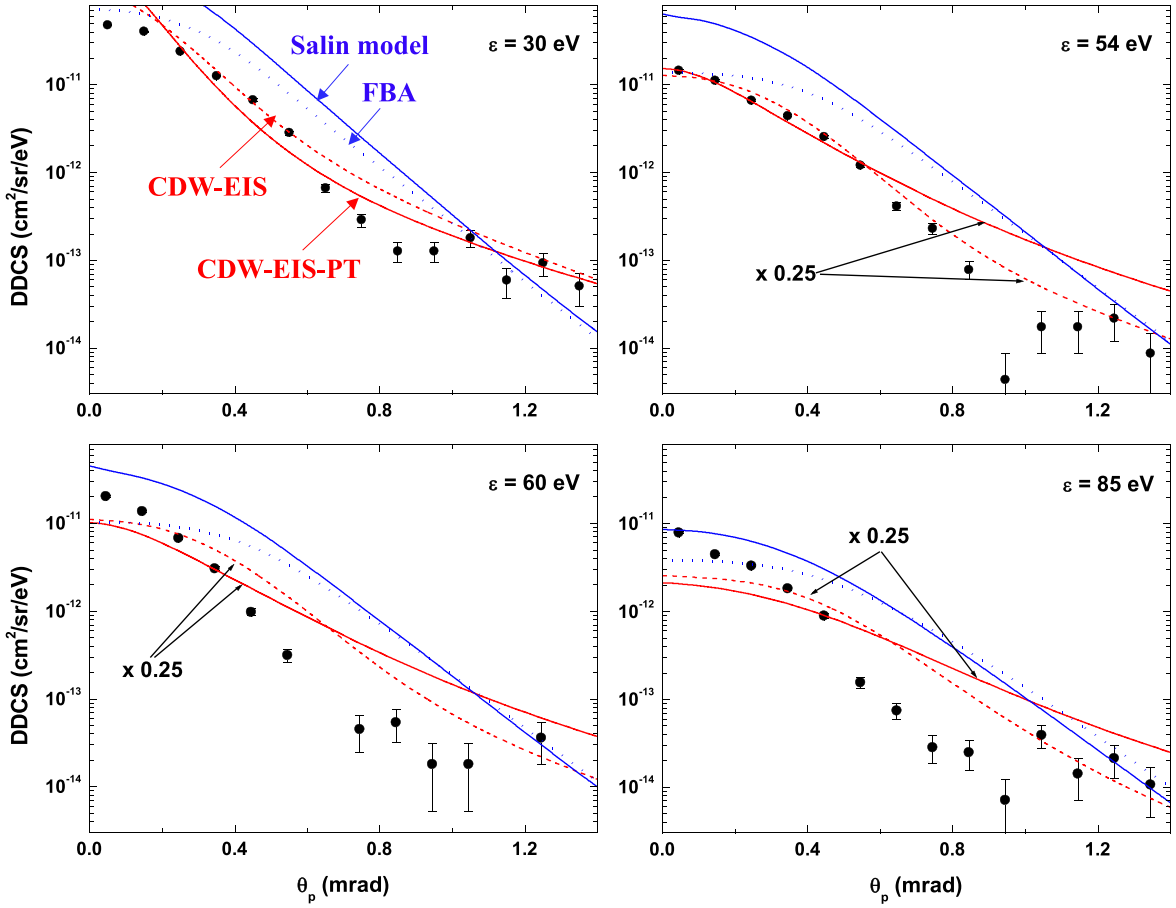

Figure 1. Double differential cross sections for ionization of Ar by 75 keV proton impact for fixed energy losses as indicated in the insets as a function of projectile scattering angle. Dotted blue curves, first Born approximation; solid blue curves, Salin model (see text); dashed red curves CDW-EIS model; solid red curves, CDW-EIS-PT model (see text).

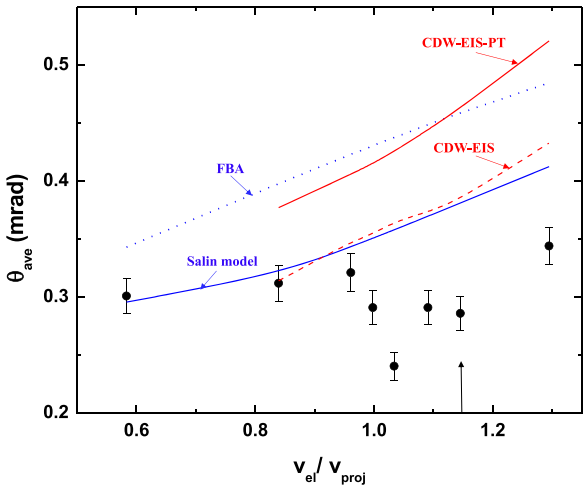

Figure 2. Average scattering angle calculated with equation (1) from the data of figure 1 as a function of the electron to projectile speed ratio. Curves as in figure 1.

In order to analyze the energy-loss dependence of the DDCS more systematically we have determined for each ε the average projectile scattering angle by

$$\theta_{\rm ave} = \int (\mathrm{DDCS}(\theta_{\rm p})\theta_{\rm p})\mathrm{d}\Omega_{\rm p} / \int (\mathrm{DDCS}(\theta_{\rm p}))\mathrm{d}\Omega_{\rm p}, \qquad (1)$$

where $\Omega_{\rm p}$ is the projectile solid angle and $\mathrm{d}\Omega_{\rm p} = 2\pi\ \sin\theta_{\rm p}\ \mathrm{d}\theta_{\rm p}$. In figure 2 $\theta_{\rm ave}$ is plotted as a function of the electron to projectile speed ratio $v_{\rm e}/v_{\rm p}$, where $v_{\rm e}$ is related to ε (in a.u.) by

$$\mathbf{v}_{\rm e} = \sqrt{2(\varepsilon - I)} \qquad (2)$$

Without any PCI effects one would expect $\theta_{\rm ave}$ to increase with increasing ε because on average an increasing energy transfer from the projectile to the target requires increasingly closer collisions. Indeed, up to about $v_{\rm e}/v_{\rm p} = 0.95$ the data follow that trend. However, near the matching speed, at about $v_{\rm e}/v_{\rm p} = 1.03$, a pronounced minimum is found. The dependence of $\theta_{\rm ave}$ on $v_{\rm e}/v_{\rm p}$ closely resembles the one observed earlier for an H_2 target [8], but it is qualitatively different compared to a He target [6]. Since I is nearly identical for Ar and H_2 (but much larger for He) this observation is consistent with the hypothesis, expressed in the introduction, that for a given projectile the importance of PCI effects may strongly depend on I.

In spite of the general similarity between the Ar and H_2 data there is also one important difference for $v_{\rm e}/v_{\rm p} > 1.1$. While for H_2 $\theta_{\rm ave}$ steeply increases in this region, for Ar it remains flat, or even has a shallow second minimum, before it starts increasing above $v_{\rm e}/v_{\rm p} > 1.2$. This difference can partly be explained by the fact that in the case of Ar the electron can be ejected from different initial states. When we determine $v_{\rm e}$

from the energy loss using equation (2) we assume that the electron is ejected from the 3p state, for which $I = 15.8$ eV, which indeed contributes about 75% to the cross section. However, the remaining 25% is due to electron ejection from the 3s state, with an ionization potential of 29.2 eV. In figure 2 the matching speed for these electrons occurs at $v_e/v_p = 1.15$ calculated with the 3p ionization potential (indicated by the arrow).

The blue dotted curves in figures 1 and 2 show the results of calculations based on the first Born approximation (FBA). Since the FBA does not account for any higher-order contributions, it shows what one would expect if PCI effects (and effects due to the PT interaction) were not present at all. Indeed, here θ_{ave} just monotonically increases with increasing v_e/v_p. The solid blue curves show the results of a model (which we call the Salin model) in which the FBA transition amplitude was multiplied by the factor $1/|\mathbf{v_e}-\mathbf{v_p}|$ to account for PCI effects in an ad hoc approach [30]. Since this factor maximizes for $\mathbf{v_e}-\mathbf{v_p} = 0$, it should considerably enhance the DDCS compared to the FBA results near $\theta_p = 0$, especially at the cusp energy. Indeed, in the Salin model the cross sections in this angular range are increased by as much as a factor of 5 (depending on ε) compared to the FBA results. This is also reflected in figure 2 by a much reduced θ_{ave} across the entire v_e/v_p range, showing that PCI effects are quite important at all ε. Considering the simplicity of this model, it was surprisingly successful in describing double differential data and the dependence of θ_{ave} on v_e/v_p for p + He collisions [6]. Very good agreement was also achieved, even in magnitude, by a more sophisticated model accounting for PCI effects in terms of a distorted wave approach [31]. However, for the present data for Ar major discrepancies between the Salin model and the experimental data are quite evident. The measured cross sections are not even qualitatively reproduced, θ_{ave} is systematically overestimated for $v_e/v_p > 0.9$, and no minimum is found near $v_e/v_p = 1$. Instead, only a slight change of slope is observed around $v_e/v_p = 0.9$.

The red dashed curves in figures 1 and 2 show our continuum distorted wave—eikonal initial state (CDW-EIS) calculations, which does not include the PT interaction. However, PCI effects are accounted for in terms of a Coulomb factor in the final-state wavefunction describing the ejected electron in the field of the scattered projectile and by an eikonal phase in the entrance channel. The solid red lines represent a CDW-EIS model, which treats the PT interaction in terms of an eikonal phase in the final-state wave function. We refer to this model as CDW-EIS-PT. It accounts for both interaction sequences leading to PCI effects, while in the CDW-EIS model only the sequence V_{Pe}–V_{eT}–V_{Pe} is included. In both models, ionization from the initial 3s and 3p states of Ar were considered. The CDW-EIS-based approaches employed in our calculations refer to the post version (for more details see [32]). The initial Ne and Ar states (both, s and p states) are modeled employing Slater orbitals, with the parameters computed and optimized using the Roothan–Hartree–Fock method [33]. In the shape of the θ_p-dependence of the DDCS (figure 1) considerably improved agreement with the experimental data compared to the FBA model and

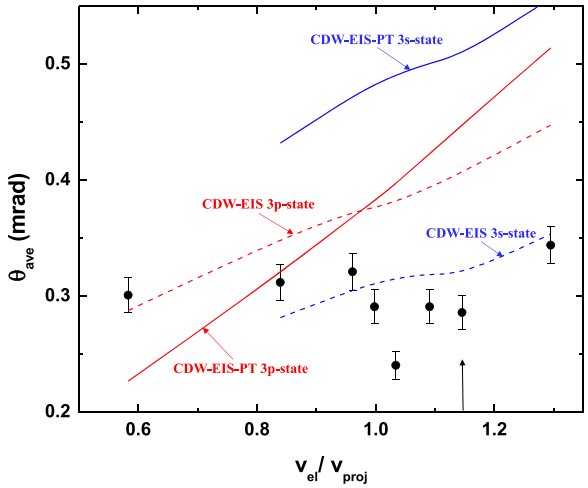

Figure 3. Same as figure 2, but curves are: dashed blue curve, CDW-EIS calculation for electron ejection from the 3s state; solid blue curve, CDW-EIS-PT calculation for ejection from the 3s state; dashed red curve, CDW-EIS calculation for electron ejection from the 3p state; solid red curve, CDW-EIS-PT calculation for ejection from the 3p state.

to the Salin model is quite evident. Nevertheless, significant discrepancies remain especially at the larger energy losses. Furthermore, the overall magnitude of the DDCS is overestimated by as much as a factor of 4.

Remarkably, the measured v_e/v_p-dependence of θ_{ave} is considerably better reproduced by the CDW-EIS than by the CDW-EIS-PT calculations. Although the CDW-EIS-PT model contains both PCI interaction sequences, it actually leads to larger θ_{ave} than the CDW-EIS model. One might be tempted to take this as an indication that the V_{Pe}–V_{PT}–V_{Pe} sequence is not adequately described by the CDW-EIS-PT model. However, it should be noted that there is another possible explanation. If the V_{Pe}–V_{PT}–V_{Pe} sequence, which represents a 3rd-order mechanism, is important, it seems plausible that the 2nd-order sequence V_{Pe}–V_{PT} is even more important. Here, one would expect that the PT interaction has a broadening effect on the projectile angular distribution which is not counteracted by the focusing effect of a subsequent second projectile–electron interaction. Therefore, the overestimation of θ_{ave} by the CDW-EIS-PT model could be due to an overestimation of this second-order sequence. This explanation is supported by the observation that for $v_e/v_p > 1.1$ θ_{ave} obtained from this approach is even larger than in the FBA calculation.

Before returning to the discussion of the role of the PT interaction after presenting the data for the Ne target, we fill first analyze the role of ionization from the 3s state of Ar. These contributions are included in the calculations, but yet the theoretical v_e/v_p-dependence of θ_{ave} shows an increase after $v_e/v_p = 1$ instead of the flat behavior observed in the experimental data. To analyze the dependence of PCI effects on the initial target state in more detail in figure 3 we replot the data of figure 2 in comparison with the CDW-EIS (dashed curves) and CDW-EIS-PT (solid curves) calculations for the 3s (blue curves) and 3p (red curves) states separately. Here,

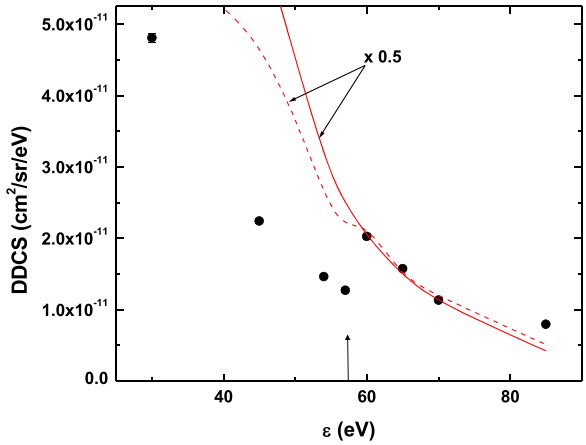

Figure 4. Double differential energy loss spectrum for 75 keV p + Ar collisions and fixed scattering angle of 0. Curves as in figure 1.

too, no clear minimum is found for either state at the respective matching speed. However, at least for the 3s state a plateau near the matching speed (indicated by the arrow in figure 3) can be seen in the CDW-EIS calculation. For the 3p state a slight hint of such a plateau is barely visible around $v_e/v_p = 1$. In the CDW-EIS-PT such a plateau is only found for the 3s state. Furthermore, for the 3s state θ_{ave} calculated with the CDW-EIS model is considerably smaller than for the 3p state across the entire v_e/v_p range. In contrast, the CDW-EIS-PT model yields larger θ_{ave} for the 3s state. These observations suggest the following: (a) the second-order sequence involving the PT interaction is stronger for the 3s state, which due to the larger ionization potential is the expected behavior. (b) Overall, in the CDW-EIS model PCI effects are much more pronounced for the 3s state, which is in accord with the expectation that such effects should become stronger with increasing I.

As mentioned in the introduction, PCI effects in ion-atom collisions were first observed in double differential ejected electron energy spectra for emission angles of 0° [2] in the form of the cusp peak. However, the intensity of the cusp peak decreases rapidly with even a small departure from a 0° emission angle and is usually not observed in cross sections integrated over all electron emission angles. In figure 4 we show DDCS for a fixed projectile scattering angle of $\theta_p = 0$ as a function of the projectile energy loss ε. Here, a peak structure a few eV above the cusp energy (indicated by the arrow) is visible. To the best of our knowledge, this spectrum represents the first observation of a cusp peak in cross sections integrated over all electron emission angles. In the CDW-EIS model (dashed curve in figure 4) PCI does not lead to a fully resolved cusp peak, but a pronounced 'shoulder structure' is visible at about the same energy as the cusp peak in the experimental data. In contrast, no structure at all is found in the CDW-EIS-PT calculation. The observation that in the CDW-EIS model the cusp structure is much less pronounced than in the measured spectrum is a strong indication that the V_{Pe}–V_{eT}–V_{Pe} sequence is not enough to fully describe PCI effects. The observation that the structure becomes even weaker in the CDW-EIS-PT model reinforces the hypothesis that the 2nd order V_{Pe}–V_{PT} sequence is overestimated and overshadows PCI effects due to the 3rd order V_{Pe}–V_{PT}–V_{Pe} sequence.

We now turn to the presentation and analysis of the data for the Ne target. Here, too, DDCS were obtained for eight energy losses and the cross sections are shown for $\varepsilon = 40$, 60, 63, and 85 eV as a function of θ_p in figure 5, where $\varepsilon = 63$ eV is closest to the cusp energy. The shape of the θ_p-dependence of the DDCS is very well reproduced by the CDW-EIS calculation (dashed red curve) for $\varepsilon = 40$ eV, but at large θ_p the agreement with experiment gets worse with increasing ε. Furthermore, as in the case of the Ar target, the inclusion of the PT interaction (solid red curve) does not lead to any improved agreement.

In figure 6 θ_{ave} is plotted as a function of v_e/v_p. Without any PCI one would expect θ_{ave} to be generally larger for Ne than for Ar because to eject the more tightly bound electrons in Ne on average requires a closer collision. Instead, up to about $v_e/v_p = 1$ θ_{ave} is actually considerably smaller. However, in contrast to Ar, only a very shallow minimum, if any at all, is observed near the matching speed and generally θ_{ave} shows only a very weak dependence on v_e/v_p. This behavior is very well reproduced by the CDW-EIS calculation, apart from an overall overestimation of θ_{ave} by about 20%. The CDW-EIS-PT approach also reproduces the shape of the dependence of θ_{ave} on v_e/v_p fairly well, but here the magnitude is too large by about a factor of 2. For Ne neither model seems to predict that PCI effects are particularly pronounced at the matching speed. However, for the double differential energy loss spectrum for $\theta_p = 0$, plotted in figure 7, a different picture emerges. In the experimental data a much weaker cusp peak than for the Ar target is observed. The opposite trend is found in the CDW-EIS model: the 'shoulder structure' in the Ar calculation at the cusp energy is turned into a peak structure in the Ne calculation. Even the CDW-EIS-PT model now predicts a 'shoulder structure'.

Along with data taken previously for H, H_2 [8], and He [6] the results presented here for Ne and Ar make possible a more systematic analysis of the dependence of PCI effects on the target properties. Figure 8 shows θ_{ave} for v_e/v_p fixed at 0.7 (open symbols) and 1 (closed symbols) as a function of the ionization potential of these five targets. Here, θ_{ave} was interpolated where data do not exist at the corresponding exact values of v_e/v_p. At $v_e/v_p = 0.7$ the decreasing trend of θ_{ave} with increasing I up to 22 eV shows that at least for relatively small I PCI effects become more important with increasing bond strength of the electrons in the initial target state. The increase of θ_{ave} above $I = 22$ eV might be due to a reversal of this dependence of PCI on I. However, a more likely explanation is that the broadening effect of the 2nd order interaction sequence V_{Pe}–V_{PT} on the projectile angular distribution is larger than the focusing effect of PCI for I larger than approximately 22 eV. A very different dependence of θ_{ave} on I is observed for $v_e/v_p = 1$, where θ_{ave} increases monotonically. This behavior is partly due to the broadening effect of the V_{Pe}–V_{PT} sequence and the general tendency (without PCI) that a larger energy transfer requires a closer collision. However, since for $v_e/v_p = 0.7$ θ_{ave} actually

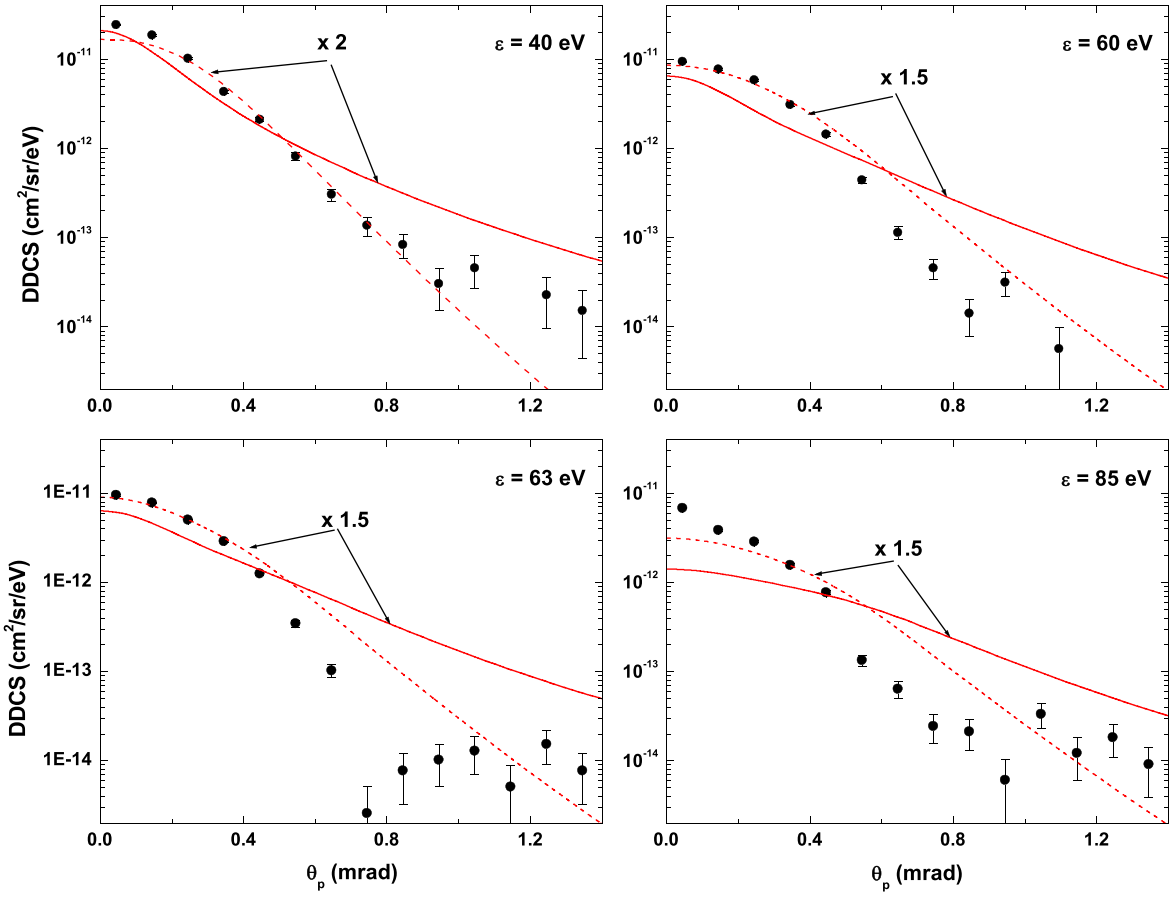

Figure 5. Same as figure 1, but for ionization of Ne.

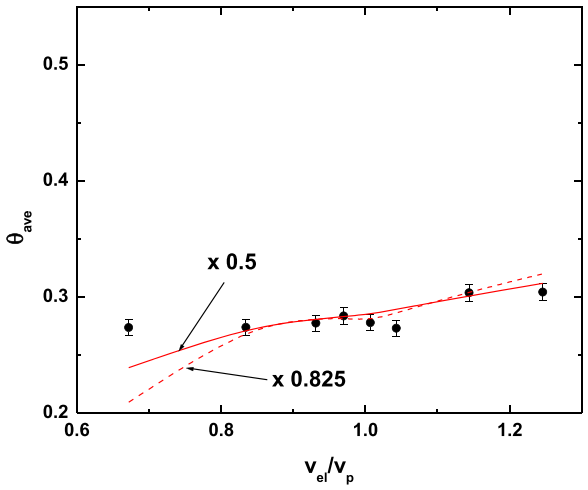

Figure 6. Same as figure 2, but for ionization of Ne.

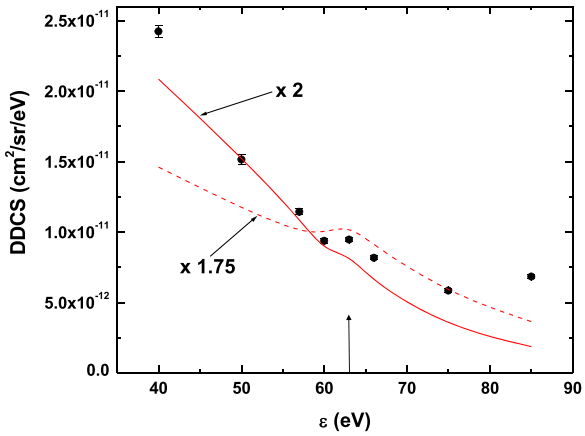

Figure 7. Same as figure 4, but for ionization of Ne.

decreases up to $I = 22$ eV the monotonic increase for $v_e/v_p = 1$ shows that here the dependence of PCI effects on I is either significantly weaker than for $v_e/v_p = 0.7$ or that they even decrease with increasing I.

Apart from the ionization potential the various targets also differ in the initial state wavefunction of the active electron. To investigate potential effects of the wavefunction on PCI effects we performed CDW-EIS-PT test calculations changing the initial state for a given target, but keeping I unchanged by adjusting the effective nuclear charge. In figure 9 we show the calculated θ_{ave} as a function of v_e/v_p for the He target in comparison with the experimental data. Here, the blue curve represents the test calculation with a 3p initial state and the red curve the 'proper' calculation with a 1s initial state. The 3p state in the test calculation was chosen because it mostly contributes to ionization of Ar, where a pronounced minimum was found in the experimental θ_{ave} at $v_e/v_p \approx 1$. The 'proper' calculation is qualitatively in very good agreement with the experimental data as it correctly predicts the change of slope around $v_e/v_p = 1$. Quantitatively, there are some discrepancies in the region

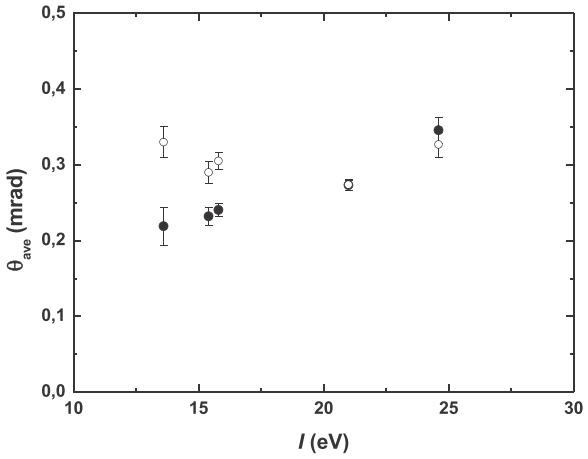

Figure 8. Average scattering angle calculated with equation (1) from the data of figure 1 for fixed v_e/v_p as a function of the target ionization potential. Open symbols, $v_e/v_p = 0.7$; closed symbols, $v_e/v_p = 1$.

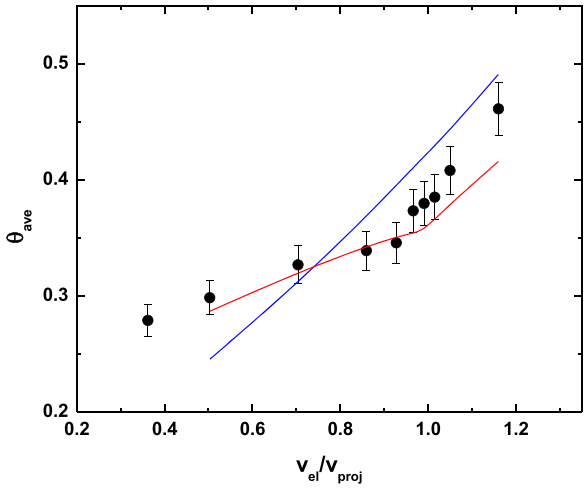

Figure 9. Same as figure 2, but for ionization of He. Curves: red solid line, CDW-EIS-PT model using a 'proper' 1s initial state and ionization potential of 24. 6 eV; blue line, CDW-EIS-PT test calculation using a 3p initial state and 'proper' ionization potential of 24. 6 eV.

$v_e/v_p > 1$, however, they do not exceed 10% of the measured θ_{ave}. In contrast, the test calculation does not even reproduce the experimental data qualitatively. The comparison between both calculations shows that the CDW-EIS-PT model predicts a significant impact of the initial state wavefunction on the width of the DDCS. However, this model cannot explain the qualitative difference between θ_{ave} for the He and Ar targets in terms of the initial state.

In figure 10, θ_{ave} is plotted versus v_e/v_p for the Ar target again comparing the experimental data to the 'proper' calculation (i.e. 3s and 3p initial states, blue curve) and a test calculation using a 1s initial state, but keeping the ionization potential at 15.8 eV (red curve)[3]. Here, too, significant differences between both calculations are found which, however,

[3] Note that this can also be viewed as a test calculation for the He target using a proper initial state, but a modified ionization potential.

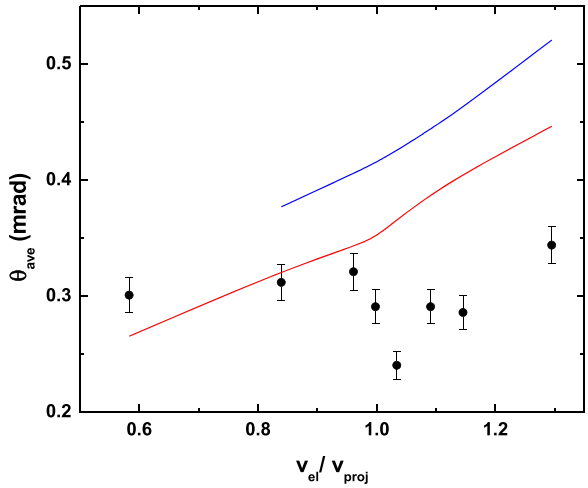

Figure 10. Same as figure 2, but curves are: blue solid line, CDW-EIS-PT model using 'proper' 3p initial state and ionization potential of 15.8 eV; red line, CDW-EIS-PT test calculation using a 1s initial state and 'proper' ionization potential of 15.8 eV.

are mostly of quantitative nature. The test calculations shows a slight change in slope at $v_e/v_p \approx 1$ not seen in the 'proper' calculation, but overall the shape is quite similar. Nevertheless, the differences in magnitude show that for the Ar target, too, the CDW-EIS-PT model predicts a significant impact of the initial state wavefunction on PCI effects. However, the test calculation is actually closer to the experimental data than the proper calculation. Therefore, the prediction by theory regarding the influence of the wavefunction are not confirmed by experiment and no conclusions regarding the effect of the initial state on PCI effects can be drawn.

Conclusions

We have measured and calculated double differential cross sections for ionization of Ne and Ar by 75 keV proton impact for a large range of projectile energy losses. Along with data taken previously for H, H_2, and He this made possible a systematic analysis on how PCI effects depend on the target ionization potential. To this end, the average projectile scattering angle was determined as a function of the ejected electron to projectile speed ratio for each target. For all targets a mutual focusing effect between the projectile and the electron caused by PCI was observed. Furthermore, for the H, H_2, and Ar targets (and possibly for Ne), a minimum in the average scattering was found at $v_e/v_p \approx 1$, indicating that here PCI effects maximize. Signatures of PCI were also observed, at least for the Ar target, in the double differential electron energy spectrum if the projectile scattering angle is fixed at 0. There, a peak structure (the so-called cusp peak) was found at an electron energy corresponding to $v_e/v_p \approx 1$. Previously, the cusp peak was not observed in any spectra if the electron ejection angle was not fixed at 0.

The observations that the minimum in the average scattering angle near $v_e/v_p = 1$ becomes more pronounced with decreasing I seems to suggest that PCI effects become stronger with decreasing I. However, factors other than the

ionization potential have to be considered. Most importantly, apart from PCI, effects due to second-order contributions involving the projectile—residual target ion interaction are also expected to depend on I and to lead to an increasing broadening of the projectile angular distribution if not compensated by the focusing due to PCI. Finally, the dependence of the strength of PCI effects on I depends on v_e/v_p. For values significantly smaller than 1 our data clearly show that PCI becomes increasingly important with increasing I. However, the observation that the minimum of θ_{ave} near $v_e/v_p = 1$ becomes more pronounced with decreasing I shows that in this region the dependence of PCI effects on I becomes substantially weaker and it may even be reversed.

Theoretically, data taken previously for He were reproduced very well [32]. However, for the heavier targets Ne and Ar the same approach yields substantial discrepancies. Some of the qualitative features observed in the experimental data are found in the calculations. For example, a narrowing effect on the projectile angular distribution by PCI and the presence of a cusp peak in the double differential energy spectra if the scattering angle is fixed at 0 are reproduced. However, quantitatively large differences to the data are found, especially in the average scattering angle which is significantly larger than in experiment. This discrepancy is probably due to an overestimation of second-order contributions involving the projectile—residual target ion interaction. Furthermore, theory predicts a dependence of PCI effects on the initial state which is not supported by experiment. Overall, further theoretical developments for heavy targets are clearly needed.

From an experimental point of view it would be highly desirable to determine the projectile energy loss and the ejected electron energy in high resolution. This would allow to separate ejection of the electron from different initial target states. The CDW-EIS model, with and without PT interaction, predicts a substantially different behavior of PCI effects for s and p states of the valence shell. Unfortunately, with our current set-up such measurements cannot be performed because the ejected electrons are not detected and the momentum resolution in the recoil ions for heavy targets is not sufficient to determine the electron energy from the conservation laws.

Acknowledgments

This work was supported by the National Science Foundation under grant nos. PHY-1703109 and PHY-1505819. M F C is grateful for support from the 'Advanced research using high intensity laser produced photons and particles' project (CZ.02.1.01/0.0/0.0/16 019/0000789) from the European Regional Development Fund (ADONIS).

ORCID iDs

M Schulz https://orcid.org/0000-0002-6336-5491

References

[1] Rudd M E, Kim Y-K, Madison D H and Gallagher J W 1985 *Rev. Mod. Phys.* **57** 965
[2] Crooks G B and Rudd M E 1970 *Phys. Rev. Lett.* **25** 1599
[3] Tribedi L C, Richard P, Dehaven W, Gulyás L, Gealy M W and Rudd M E 1998 *Phys. Rev.* A **58** 3619
[4] Sarkadi L, Palinkas J, Köver A, Berenyi D and Vajnai T 1989 *Phys. Rev. Lett.* **62** 527
[5] Schmitt W, Moshammer R, O'Rourke F S C, Kollmus H, Sarkadi L, Mann R, Hagmann S, Olson R E and Ullrich J 1998 *Phys. Rev. Lett.* **81** 4337
[6] Vajnai T, Gaus A D, Brand J A, Htwe W, Madison D H, Olson R E, Peacher J L and Schulz M 1995 *Phys. Rev. Lett.* **74** 3588
[7] Laforge A C, Egodapitiya K N, Alexander J S, Hasan A, Ciappina M F, Khakoo M A and Schulz M 2009 *Phys. Rev. Lett.* **103** 053201
[8] Schulz M, Laforge A C, Egodapitiya K N, Alexander J S, Hasan A, Ciappina M F, Roy A C, Dey R, Samolov A and Godunov A L 2010 *Phys. Rev.* A **81** 052705
[9] Schulz M, Moshammer R, Fischer D, Kollmus H, Madison D H, Jones S and Ullrich J 2003 *Nature* **422** 48
[10] Schulz M, Moshammer R, Perumal A N and Ullrich J 2002 *J. Phys.* B **35** L161
[11] Maydanyuk N V, Hasan A, Foster M, Tooke B, Nanni E, Madison D H and Schulz M 2005 *Phys. Rev. Lett.* **94** 243201
[12] Schulz M *et al* 2013 *Phys. Rev.* A **88** 022704
[13] Hasan A *et al* 2016 *J. Phys.* B **49** 04LT01
[14] Hasan A, Sharma S, Arthanayaka T P, Lamichhane B R, Remolina J, Akula S, Madison D H and Schulz M 2014 *J. Phys.* B **47** 215201
[15] Gassert H *et al Phys. Rev. Lett.* **116** 0732012016
[16] Dhital M *et al* 2019 *Phys. Rev.* A submitted
[17] Chuluunbaatar O, Zaytsev S A, Kouzakov K A, Galstyan A, Shablov V L and Popov Y V 2017 *Phys. Rev.* A **96** 042716
[18] Godunov A L, Whelan C T and Walters H R J 2008 *Phys. Rev.* A **78** 012714
[19] Belkić D 1991 *Phys. Rev.* A **43** 4770
[20] Fiol J, Rodríguez V D and Barrachina R O 2001 *J. Phys.* B **34** 933
[21] Madison D H, Fischer D, Foster M, Schulz M, Moshammer R, Jones S and Ullrich J 2003 *Phys. Rev. Lett.* **91** 253201
[22] Pedlow R T, O'Rourke S F C and Crothers D S F 2005 *Phys. Rev.* A **72** 062719
[23] Ciappina M F and Rivarola R D 2008 *J. Phys.* B **41** 015203
[24] Voitkiv A B 2017 *Phys. Rev.* A **95** 032708
[25] McGovern M, Assafrao D, Mohallem J R, Whelan C T and Walters H R J 2010 *Phys. Rev.* A **81** 042704
[26] Pindzola M S, Colgan J, Robicheaux F, Lee T G, Ciappina M F, Foster M, Ludlow J A and Abdel-Naby S A 2016 *Ad. At. Mol. Opt. Phys.* **65** 291
[27] Abdurakhmanov I B, Bailey J J, Kadyrov A S and Bray I 2018 *Phys. Rev.* A **97** 032707
[28] Gaus A D, Htwe W, Brand J A, Gay T J and Schulz M 1994 *Rev. Sci. Instrum.* **65** 3739
[29] Rudd M E, Kim Y-K, Madison D H and Gay T J 1992 *Rev. Mod. Phys.* **64** 441
[30] Salin A 1969 *J. Phys.* B **2** 631
[31] Rodriguez V D and Barrachina R O 1998 *Phys. Rev.* **A57** 215
[32] Ciappina M F, Cravero W R and Garibotti C R 2003 *J. Phys.* B **36** 3775
[33] Clementi E and Roetti C 1974 *At. Data Nucl. Data Tables* **14** 177